A Cavitation Susceptibility Meter With Optical Cavitation Monitoring—Part One: Design Concepts

L. d'Agostino[1]

A. J. Acosta

California Institute of Technology, Pasadena, Calif. 91125

This work is concerned with the design of a Cavitation Susceptibility Meter based on the use of a venturi tube for the measurement of the active cavitation nuclei concentration in water samples as a function of the applied tension. The operation of the Cavitation Susceptibility Meter is analyzed and the main considerations leading to the proposed design are illustrated and critically discussed. The results of this analysis indicate that the operational range is mainly limited by nuclei interference, flow separation and saturation (choking), and suggest to develop a Cavitation Susceptibility Meter where: (a) the flow possesses a laminar potential core throughout the venturi throat section in all operational conditions; (b) the pressure at the venturi throat is determined from the upstream pressure and the local flow velocity; (c) the detection of cavitation and the measurement of the flow velocity are carried out optically by means of a Laser Doppler Velocimeter; (d) a custom-made electronic Signal Processor incorporating a frequency counter is used for real time data generation and temporary storage; (e) a computerized system performs the final acquisition and reduction of the data.

1 Introduction

It has long been recognized (Knapp et al., 1970) that the occurrence of cavitation is controlled by weak spots, generically called "nuclei", which act as preferential points for the onset of liquid rupture and significantly reduce the tensile strength of the liquid. The inception, development, and scaling of cavitation are greatly influenced by the concentration of cavitation nuclei which become active at a given pressure level. The problem of cavitation nuclei detection has received considerable attention in view of the importance of cavitation in a wide variety of technical applications (Billet, 1986; Billet, 1985). Photography, holography, acoustical and optical scattering, Coulter Counters and acoustical attenuation have all been used in the past to detect cavitation nuclei and measure their size concentration distribution. However, the tensile strength of all kinds of nuclei except microbubbles is not directly related to their size and therefore little quantitative information can be obtained from the above methods on the critical tension which makes each nucleus unstable, as required for cavitation studies. This limitation is overcome in Cavitation Susceptibility Meters (CSM), instruments first proposed by Oldenziel (Oldenziel, 1982a; Oldenziel, 1982b), where cavitation occurring in the internal flow through a venturi tube is directly monitored. Ideally, if the size of the venturi throat region and the nuclei concentration are sufficiently small, each nucleus can cavitate individually in carefully controlled conditions and the concentration of active cavitation nuclei at any given pressure can be directly measured. In the CSM developed by Oldenziel cavitation takes place in a glass venturi and is detected optically, while in other applications (Lecoffre and Bonnin, 1979; Le Goff and Lecoffre, 1983; Shen et al., 1984) stainless-steel venturi tubes are used and cavitation bubbles are recognized acoustically from the noise generated by their collapse.

Mutual interference between cavitation nuclei and saturation (choking) in the venturi throat at high nuclei concentration modify the pressure with respect to its steady noncavitating value and limit the useful operational range of CSM's. Flow separation in the diffuser and the occurrence of sheet cavitation in the throat section of the venturi tube due to the higher susceptibility of surface nuclei with respect to free stream ones also represent possible causes of malfunction in CSM's. As shown later in this paper, these difficulties are quite severe and must be carefully controlled by proper design of the CSM. On the other hand, the main advantages of CSM' consist in the capability of measuring the nuclei critical tension and concentration directly (thus eliminating the problem of the uncertain behavior of particles as cavitation nuclei), in the relative speed and convenience of data analysis and in the absence of limitations on the minimum size of cavitation nuclei that can be detected. These distinct advantages make CSM's an attractive alternative to other nuclei detection techniques for the purpose of cavitation research. The present study is part of our current work on this subject (d'Agostino, 1987; d'Agostino et al., 1989)

[1]Now at the Dipartimento di Ingegneria Aerospaziale, Universitá di Pisa, 56126 Pisa, Italy.

Contributed by the Fluids Engineering Division for publication in the JOURNAL OF FLUIDS ENGINEERING. Manuscript received by the Fluids Engineering Division July 20, 1989.

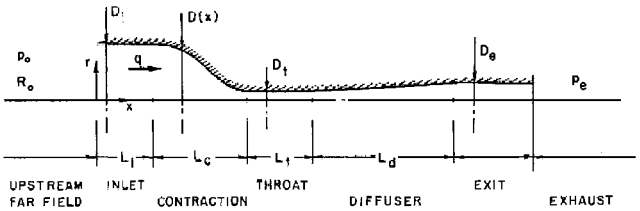

Fig. 1 Geometry and nomenclature of axisymmetric CSM venturi duct

and reports the main considerations leading to the design of the CSM recently developed at the California Institute of Technology. For conciseness the implementation and operation of the whole system are described in detail in a companion paper (d'Agostino and Acosta, 1991).

2 Bubble Dynamics and Venturi Geometry

The configuration of the axisymmetric CSM venturi pipe considered in the present study in shown in Fig. 1. The flow originates from the far field on the left (subscript 0), representing the sampled liquid, passes through the venturi and finally reaches the exhaust region on the right. Both the upstream and downstream conditions are supposed to be independent on time t. Let x be the space coordinate along the venturi centerline. A volume flux $q(t)$ of liquid with density ρ and kinematic viscosity ν flows with average axial velocity $u(x, t)$ through the venturi of local diameter $D(x)$ and cross-sectional area $A(x) = \pi D^2(x)/4$. The venturi duct is divided in five segments: a cylindrical inlet (subscript i), a contraction (subscript c), a cylindrical throat (subscript t), a diffuser (subscript d), and a cylindrical exhaust (subscript e). The length L of each segment of the duct is shown in the same figure; the inlet contraction area ratio is: $C_c = A_t/A_i$ and the diffuser expansion area ratio is: $C_e = A_e/A_t$.

By means of various assumptions and approximations, a simplified model can be derived which adequately represents the operation of CSM's in terms of a limited number of relevant parameters (see Fig. 2). The investigation of their mutual relations leads to a functional description of CSM operation which enables one to address the problem of their design in a systematic and organic way.

In cavitation research literature the liquid quality of a sample is usually expressed by means of the nuclei number concentration density distribution: $N(R_0) = -dn(R_0)/dR_0$, where

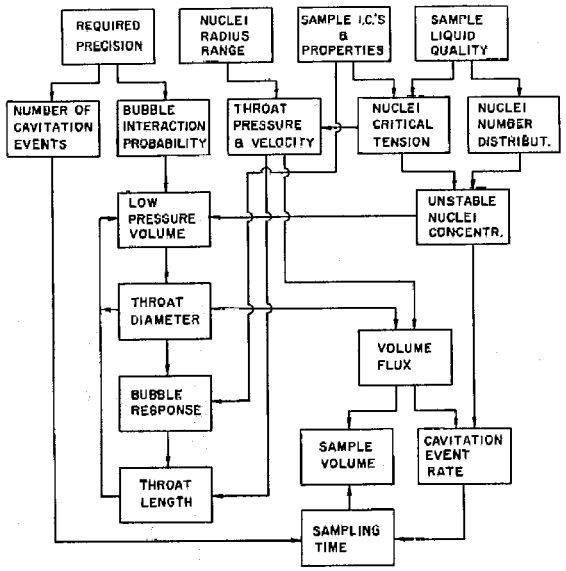

Fig. 2 Block diagram of CSM parameters

$n(R_0)$ is the number concentration of nuclei whose equilibrium radius is not smaller than R_0. The nuclei number distributions of water samples of technological interest spread in practice over a very large range and in most cases approximately follow a hypergeometric distribution (Bader, 1970). Here, for simplicity, we assume $N(R_0) = K_N/R_0^3$ and therefore $n(R_0) = K_N/2R_0^2$, with $K_N = 10^{-1}$ m^{-1}. This value is generally representative of the data from technical waters reported in the literature for the radius range from 10 to 100 μm considered in this analysis (O'Hern et al., 1988). However, errors by an order of magnitude on both sides are quite possible in practice because of the large dispersion of liquid quality data reported in the literature.

Bubble dynamics closely models cavitation from any kind of nuclei as the cavity grows bigger than the original nuclei size. We thus assume for simplicity that all the nuclei consist of equilibrium gas bubbles, whose critical tension with respect to quasi-static mechanical stability (Knapp et al., 1970) is expressed by:

$$(p_v - p)_{cr} = \frac{4S}{3R_0}\left[3\left(1 + \frac{p_0 - p_v}{2S/R_0}\right)\right]^{-1/2} \tag{1}$$

Nomenclature

A = cross-sectional area
C_c = venturi contraction coefficient
C_e = venturi expansion coefficient
C_{p_e} = exhaust pressure coefficient
D = venturi diameter
d_x, d_y, d_z = principal axes of the LDV focal ellipsoid
f = frequency, focal length, probability density distribution
f_D = Doppler frequency or its data value
K_N = nuclei number distribution parameter
L = length
L_f = detection length of a bubble or cavitation nucleus
m = index of refraction
$n(p_t)$ = concentration of nuclei with critical pressure not smaller than p_t
$n(R_0)$ = concentration of nuclei with equilibrium radius not smaller than R_0
N = integer number
$N(R_0)$ = nuclei number concentration density distribution
p = pressure
p_b = bubble external far field pressure
p_g = bubble noncondensable gas pressure
p_t = venturi throat pressure
p_u = venturi upstream pressure
Pr = probability
q = volume flux, Gaussian beam complex parameter
R = radius, bubble or cavitation nucleus radius
$1/R$ = laser beam wave front curvature
R_f = detection radius of a bubble or cavitation nucleus
$1/R_f$ = laser beam wave front curvature at the LDV focal point
Re = Reynolds number
s = LDV beam semi-separation
s_{fr} = fringe spacing
S = surface tension
t = time
t_f = detection time of a bubble or cavitation nucleus
T = temperature
T_g = Doppler gate time
u = velocity

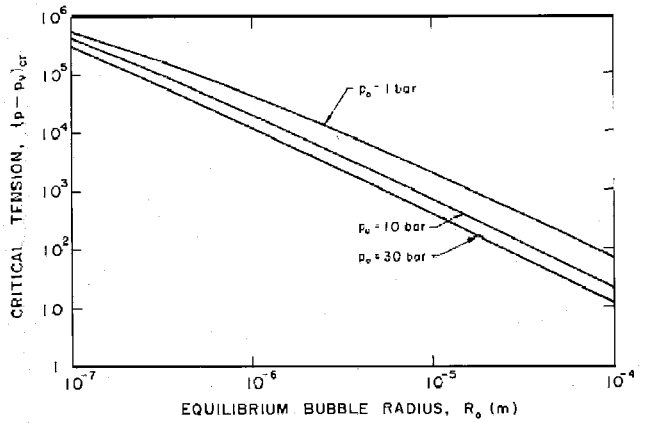

Fig. 3 Critical tension $(p - p_v)_{cr}$ of a spherical air bubble v/s its equilibrium radius R_0 in water at various pressures p_0 = 1, 10 and 30 bar and T = 20°C (surface tension S = 0.073 N/m, vapor pressure p_v = 1919 Pa, water density ρ = 1000 kg/m³).

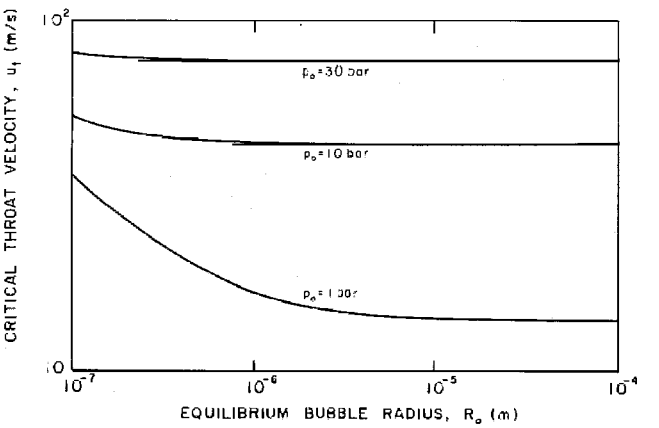

Fig. 4 Throat velocity u_t v/s equilibrium bubble radius R_0 in water at various pressures p_0 = 1, 10 and 30 bar and T = 20°C

Here p_0 and R_0 are the equilibrium pressure and radius of the bubble, p_v is the vapor pressure and S is the surface tension (see Fig. 3). The corresponding "critical" velocity at the venturi throat deduced from ideal, incompressible, one-dimensional, steady flow calculations is shown in Fig. 4. Similarly, the exhaust pressure coefficient $C_{p_e} = (p_e - p_v)/(p_0 - p_v)$ is plotted in Fig. 5 for the case p_0 = 1 bar and various expansion ratios. When the equilibrium pressure p_0 increases, the C_{p_e} curves shift to the left in the diagram. Note that, since the critical tensions of bubbles in the radius range of interest (from 10 to 100 μm) are quite small, the radius of marginally stable bubbles (critical radius) is a very sensitive function of the applied tension. If, in first approximation, dynamic effects are neglected, the above critical pressure would be representative of the cavitation pressure in the venturi throat, with several important (and unfortunate) implications for the design of CSM's. The first is that it would be virtually impossible to measure these small pressures at the throat because of inadequate sensitivity and, if done intrusively, separation and/or cavitation would surely be induced in such an extremely unstable flow. The second is that the throat pressure should be evaluated accurately to avoid large errors in the determination of the nuclei number distribution. A third consequence has to do with the problem of regulating the flow. Since the pressure

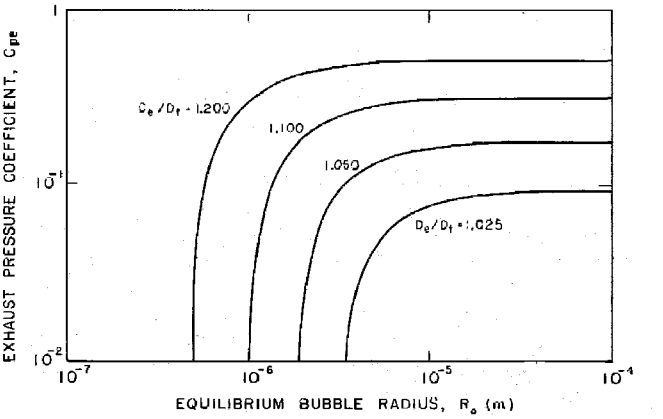

Fig. 5 Exhaust pressure coefficient $C_{p_e} = (p_e - p_v)/(p_0 - p_v)$ v/s equilibrium bubble radius R_0 in water at p_0 = 1 bar and T = 20°C for various values of the diffuser's exhaust to throat diameter ratio D_e/D_t = 1.025, 1.050, 1.100, and 1.200

upstream cannot be changed without seriously affecting the sample and therefore interfering with the liquid quality measurement, this must be done by varying the exhaust pressure. The curves of Fig. 5 for p_0 = 1 bar show that very low sensitivity

Nomenclature (cont.)

u_t = venturi throat velocity
U = velocity component measured by the LDV
V = volume
w = laser beam radius
w_f = laser beam radius at the LDV focal point
w_0 = laser beam waist radius
x = venturi axial coordinate
y = coordinate in the direction of the LDV optical axis
z = vertical coordinate normal to x and y
β = nuclei interference probability
β_d = semi-aperture angle of the venturi diffuser
δ^* = displacement boundary layer thickness
ϵ = error
θ = momentum boundary layer thickness
λ = boundary layer correlation parameter
λ_0 = wave length of LDV laser beams in air
ν = water kinematic viscosity
$\bar{\nu}_b$ = average cavitation event rate
ρ = water density
σ = standard deviation
σ^2 = variance
φ = semi-aperture angle of the LDV beams in air
ξ = Poisson distribution parameter

Subscripts

b = bubble or cavitation event
c = venturi tube contraction
cr = critical
d = venturi tube diffuser
e = venturi tube exhaust
fr = fringe
i = venturi tube inlet
0 = reference equilibrium conditions
p = particle or velocity tracer
s = sample
t = venturi tube throat
u = upstream
v = vapor
zc = zero crossing

Acronyms

CSM = Cavitation Susceptibility Meter
LDV = Laser Doppler Velocimeter

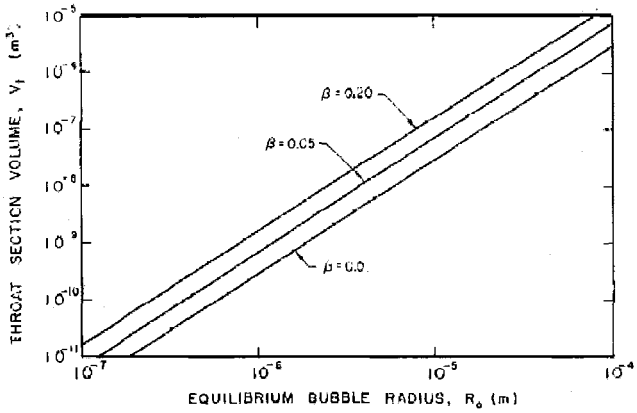

Fig. 6 CSM venturi throat section volume V_t v/s equilibrium bubble radius R_0 for $K_N = 0.001$ m^{-1} (nuclei number distribution parameter) and various values of the bubble interference probability β = 0.01, 0.05 and 0.20

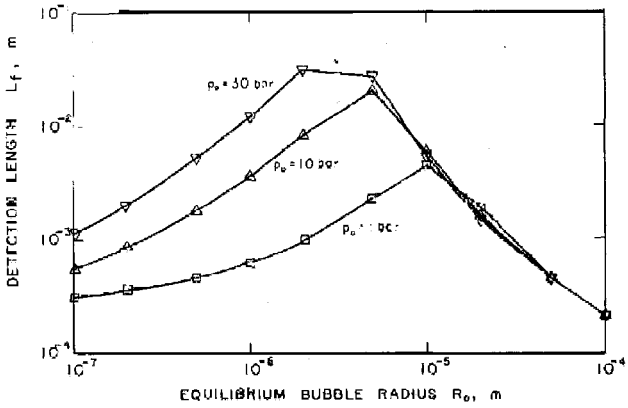

Fig. 7 Bubble detection length L_f necessary for a bubble to reach a detectable radius R_f = 150 μm v/s equilibrium bubble radius R_0 at various initial pressures p_0 = 1 bar (squares), 10 bar (upward triangles) and 30 bar (downward triangles) for T = 20°C (water temperature) and D_t = 1 mm (throat diameter)

would be obtained, unless diffusers with a very small expansion ratio were used. In practice the highly dynamic nature of cavitation in the CSM throat significantly decreases the cavitation pressure (d'Agostino et al., 1989) with respect to the value indicated by (1), but the above considerations still remain valid in a qualitative sense.

As pointed out briefly in the introduction, the problem of saturation poses a significant limitation to the operation of CSM's. It also introduces a systematic error, since the unsteady pressure perturbations due to the presence of a growing or collapsing bubble in the cavitation region of the CSM can prevent the normal growth of other neighboring nuclei. To control such an error the probability of finding more than one unstable nucleus in the throat volume V_t of the CSM must be minimized. When the nuclei concentration is uniform, the occurrence of N_b unstable nuclei in V_t is expected to follow the Poisson distribution $Pr(N_b) = \xi^{N_b}/N_b!e^{\xi}$, where $\xi = n(R_0)V_t$ is the average number of unstable nuclei in V_t. Hence, the cumulative probability of observing two or more unstable nuclei in V_t (bubble interference probability) is: $\beta = 1 - Pr(0) - Pr(1) = 1 - (1 + \xi)e^{-\xi}$. It is therefore possible to express the throat volume of the CSM as a function of the equilibrium bubble radius and of the bubble interference probability. The results of Fig. 6 show that in the radius range from 10 to 100 μm the volume of the throat section of the CSM should not exceed about 100 mm^3 if the interference error is to be reduced to an acceptable level, say less than 20 percent. In this respect a throat diameter of 1 mm ca. appears to be both feasible and adequate, therefore further considerations are based on such a choice.

The problem of the response of an isolated bubble in the throat of the CSM is now approached. The solution of such a problem is expressed in terms of the detection time t_f and detection length L_f, respectively defined as the time and the length necessary for the bubble to grow from its initial size R_0 to a final detectable radius R_f. The choice of the final radius R_f is somewhat arbitrary, since it clearly depends on the sensitivity of the method used to detect cavitation. The solution of the above problem provides a way to estimate the minimum necessary length of the throat volume, thus completing its geometrical definition. A number of assumptions are made in order to construct a simplified set of equations which nevertheless models the interactions between the bubble and the liquid. First the flow is supposed to be one-dimensional, ideal, incompressible and the relative motion of the bubble with respect to the surrounding liquid is neglected. The bubble, moving along the centerline of the duct with instantaneous position $x_b(t)$, remains spherical and its radius $R(t)$ is determined by the Rayleigh-Plesset equation (Plesset and Prosperetti, 1977; Knapp et al., 1970):

$$p_v - p_b = \rho\left[R\frac{d^2R}{dt^2} + \frac{3}{2}\left(\frac{dR}{dt}\right)^2\right] - p_g\left(\frac{R_0}{R}\right)^3 + \frac{2S}{R}$$

where S is the surface tension and diffusive and thermal effects are neglected, i.e., p_v and p_g are constant. Here p_b is the external pressure driving the bubble volume changes and it is assumed to be equal to the pressure of the liquid in the proximity of the bubble. Then, from the continuity and unsteady Bernoulli's equations for the inlet flow upstream of the bubble (subscript i) and the exit flow downstream of the bubble (subscript e):

$$q_i - q_b + 2\pi R^2\frac{dR}{dt} = 0 \tag{2}$$

$$q_e - q_b - 2\pi R^2\frac{dR}{dt} = 0 \tag{3}$$

$$-I_i\frac{dq_i}{dt} + \frac{p_i - p_b}{\rho} - \frac{1}{2}\frac{q_b^2}{A_b^2} = 0 \tag{4}$$

$$-I_e\frac{dq_e}{dt} + \frac{p_b - p_e}{\rho} + \frac{1}{2}\frac{q_b^2}{A_b^2} - \frac{q_e^2}{A_e^2} = 0 \tag{5}$$

where $A_b = A(x_b)$, p_i and p_e are constant and:

$$I_i = \int_{x_i}^{x_b}\frac{dx}{A(x)}; \quad I_e = \int_{x_b}^{x_e}\frac{dx}{A(x)}$$

Equations (2) through (5) are then transformed by introducing perturbation quantities with respect to the steady-state solution and linearized for small changes in the volume fluxes. Finally, if $I_i \simeq x_b/A_b = u_t l/A_t \ll I_i + I_e$, which is essentially equivalent to consider the dynamics of a bubble entering a semi-infinite pipe of constant cross-sectional area A_t, the perturbation and Rayleigh-Plesset equations can be reduced to the following second order differential equation for the bubble radius $R(t)$:

$$\frac{2\pi\rho u_t}{A_t}\left[2tR^2\frac{d^2R}{dt^2} + 4tR\left(\frac{dR}{dt}\right)^2 + R^2\frac{dR}{dt}\right] + \rho R\frac{d^2R}{dt^2} + \frac{3}{2}\rho\left(\frac{dR}{dt}\right)^2 - p_v - p_g\left(\frac{R_0}{R}\right)^3 + \frac{2S}{R} + p_t = 0$$

where p_t and u_t are the steady-state pressure and velocity at the throat. Note that the solution of the above equation depends on A_t, the throat cross-sectional area. The detection length $L_f = u_t t_f$, computed for a final detection radius R_f = 150 μm and a throat diameter D_t = 1 mm by numerically integrating the above equation, is shown in Fig. 7. The maximum in the results separates two regimes: in the upper radius range the inertial effects of the displaced liquid dominate, while

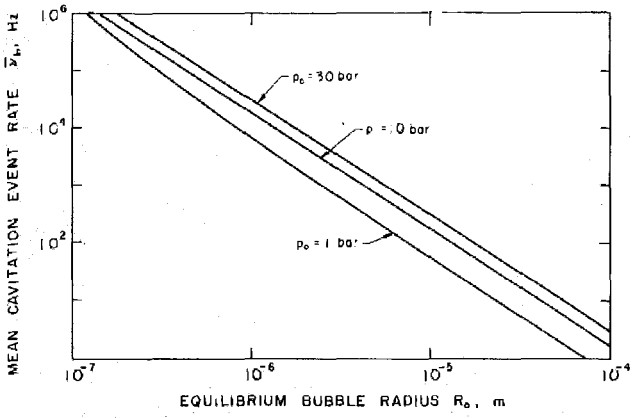

Fig. 8 Average cavitation event rate $\bar{\nu}_b$ v/s equilibrium bubble radius R_0 in water at various pressures p_0 = 1, 10 and 30 bar for D_t = 1 mm (throat diameter), K_N = 0.001 m^{-1} (nuclei number distribution parameter) and T = 20°C (water temperature)

in the lower one the effects of surface tension and bubble gas content prevail, therefore accelerating the bubble dynamic response to a change of the external pressure. Note that, in the radius range of interest, the detection length is almost independent of the equilibrium bubble pressure and that the length of the throat section should not be shorter than 5 to 10 mm. Given the throat diameter initially assumed, this choice is compatible with the need to control the bubble interference error over the nuclei radius range in consideration.

3 Unstable Nuclei Concentration and Throat Pressure Measurements

Once the throat cross-sectional area has been determined, the volume flux $q = u_t A_t$ and the mean cavitation event rate $\bar{\nu}_b = qn(R_0)$ can be computed. Results of Fig. 8 for a throat diameter D_t = 1 mm indicate that in the radius range from 10 to 100 μm as many as maybe a thousand cavitation events per second are to be expected. In steady-state conditions, if the liquid quality of the sample is constant and the cavities do not appreciably interfere with each other, the occurrence of cavitation at the venturi throat is described by a Poisson process with average arrival time $1/\bar{\nu}_b$. Then, the probability of observing N_b cavities during the time t is expressed by $Pr(N_b) = (\bar{\nu}_b t)^{N_b}/N_b! e^{\bar{\nu}_b t}$ and the probability density distribution of the time interval t between successive cavitation events follows the exponential distribution $f(t) = \bar{\nu}_b e^{-\bar{\nu}_b t}$. The agreement of the observed distribution of cavitation delay times with the above theoretical one provides a rational and quantitative way to assess the importance of interference effects among the cavities in the CSM venturi flow and to introduce corrections when appropriate (d'Agostino and Acosta, 1991). Note that a large portion of cavitation events will occur with a separation in time considerably smaller than the average arrival time $1/\bar{\nu}_b$. Therefore the CSM data acquisition system must be designed to handle as many as, say, order of ten thousand cavitation events per second for a reliable measurement of the water quality to be made. In addition, it also must record the arrival times with comparable precision, if the importance of cavitation interference effects is to be assessed from consideration of the delay time statistics.

For a given pressure at the throat, the corresponding concentration of unstable nuclei can be estimated from the count N_b of the cavitation bubbles observed during the sampling time t_s. Since t_s can be conveniently measured, the problem of estimating $\bar{\nu}_b$ now reduces to the estimation of the Poisson parameter $\xi = \bar{\nu}_b t_s$. It is known from the theory of probability distributions, (Browlee, 1960), that the best estimator of the Poisson parameter ξ is the observed frequency N_b, whose expected value and variance are respectively: $\overline{N}_b = \sigma^2_{N_b} = \xi$. Thus, the estimated root mean square relative error in the measurement of ξ and of any other linearly related quantity such as $\bar{\nu}_b$, $n(R_0)$ and $N(R_0)$ is $\epsilon = 1/\sqrt{N_b}$. The sampling time $t_s = 1/\bar{\nu}_b \epsilon^2$ and liquid sample volume $V_s = A_t u_t t_s$ necessary for one single measurement of unstable nuclei concentration of acceptable precision (say, $\epsilon = 0.20$) are found to be at most of the order of 10 dm^3 and 10 s, respectively. Clearly, the overall sampling time and volume of liquid necessary for the evaluation of the nuclei number distribution will depend on the total number of points where the measurement of the unstable nuclei concentration is carried out. Finally, the unstable nuclei concentration is estimated as $n(R_0) = N_b/V_s$, with standard deviation $\sigma_n = \sqrt{N_b}/V_s$.

In existing CSM's cavitation detection has been made either optically (Oldenziel, 1982a; Oldenziel, 1982b; Oldenziel et al., 1982; Ito and Oba, 1980) or acoustically (Lecoffre and Bonnin, 1979; Le Goff and Lecoffre, 1983; Shen et al., 1984) from the noise generated by the rapid volume changes of the cavities and in particular by their collapses. Acoustical detection is relatively simple and has the distinct advantage of not requiring optical access to the cavitation region. However, rebounds frequently occur in practice during the collapse of cavitation bubbles, possibly leading to spurious counts due to multiple acoustical signals from the same original cavity. Optical detection is clearly preferable whenever feasible because it safely locates the occurrence of cavitation in space, thus eliminating the possibility of spurious multiple counts, and preserves the information on the arrival time of cavitation events, which represents a powerful diagnostic tool in monitoring the operation of CSM's. In addition, the possibility of direct optical observation of cavitation in the venturi is an important advantage of optical methods for cavitation detection.

It was previously mentioned that one of the most difficult problems of CSM's consists in measuring the throat pressure with the required precision. Since direct methods appear to be impossible, indirect methods must be used. Most naturally a representative value of the inception pressure at the venturi throat may be deduced from the measurements of the upstream pressure and of the throat velocity using Bernoulli's equation for ideal, incompressible, steady flow:

$$p_t = p_u - \frac{1}{2}\rho u_t^2 (1 - C_c^2) \qquad (6)$$

An unavoidable problem associated with this technique is that the throat pressure, being inherently small compared to the inlet pressure and kinetic pressure drop, is expressed as the difference of two almost equal quantities. Thus, small relative errors in the evaluation of these quantities lead to a much larger relative error for the throat pressure.

In existing CSM's, (Oldenziel, 1982a; Oldenziel, 1982b; Oldenziel et al., 1982; Godefroy et al., 1981; Le Goff and Lecoffre, 1983; Shen et al., 1984) the velocity measurement was carried out either in the upstream or downstream sections of the duct, relatively far from the venturi throat. This method appears to be rather unsatisfactory for various reasons. First, any intrinsic error in the measurement of the velocity or due to inaccurate estimate of boundary layer effects is amplified proportionally to the reciprocal of the venturi contraction ratio when the throat velocity is derived by means of continuity arguments. This limitation is particularly severe since in CSM's the contraction ratio should be as small as possible in order not to appreciably affect the conditions of the sampled liquid during its flow to the test section. Moreover, it is generally necessary to make the inlet line longer, which is also likely to affect the conditions of the sampled liquid, especially when a second venturi of smaller contraction ratio is used to monitor the velocity. These difficulties are overcome if the velocity measurement is carried out at the throat. In consideration of the

extreme instability of the flow, the use of a Laser Doppler Velocimeter (LDV) seems to be the best solution.

The error analysis of this measurement can be easily developed if the two independent variables p_u and u_t are assumed to be normally distributed about their expected values $\bar{p}_u$ and $\bar{u}_t$ with variances $\sigma^2_{p_u}$ and $\sigma^2_{u_t}$. Standardizing p_u and u_t and using the properties of the moments of the standard normal distribution (Browlee, 1960), one obtains the following expressions for the expected value and the variance of p_t:

$$\bar{p}_t = \bar{p}_u - \frac{1}{2}\rho(1 - C_c^2)(\bar{u}_t^2 + \sigma^2_{u_t})$$

$$\sigma^2_{p_t} = \sigma^2_{p_u} + \rho^2(1 - C_c^2)^2\sigma^2_{u_t}\left(\bar{u}_t^2 + \frac{\sigma^2_{u_t}}{2}\right)$$

Note the "shift" due to the dispersion of the measured velocity together with the quadratic nature of equation (6).

4 Viscous Effects

For the pressure to be correctly deduced from velocity measurements, the presence of a laminar potential core at the CSM throat must be demonstrated. Viscous effects have therefore been estimated by matching an axisymmetric laminar boundary layer (White, 1974) to the quasi one-dimensional ideal flow solution based on the duct geometry. The assumption of laminar flow in the venturi is justified by the low value of the Reynolds number at the inlet ($\mathrm{Re}_i = u_i D_i/\nu \simeq 1500$) and, further downstream where the Reynolds number increases beyond the transition value, by the effect of the steep contraction which tends to laminarize the flow by drastically reducing preexisting velocity fluctuations. The turbulent transition length for a flat plate with equal free stream velocity is of the order of 20 cm and it seems likely that it would not be shorter for the guided flow in the CSM venturi. Thus there is strong reason to believe that at least the noncavitating flow remains laminar throughout the whole venturi. In the boundary layer computation the duct profile has been assumed to be continuous with continuous first and second derivatives, as required from fluid mechanical considerations to avoid separation. In the contraction and the transitions at the inlet and outlet of the diffuser the duct radius was supposed to have sinusoidal second derivative in the streamwise direction. The inlet and throat sections were taken to be cylindrical and the center part of the diffuser to be conical, of given semi-aperture angle β_d. The boundary layer displacement and momentum thicknesses δ^* and θ for a typical venturi with inlet Reynolds $\mathrm{Re}_i = 1400$ (the lowest expected value during operation) are summarized in Fig. 9, where they are normalized with respect to the local duct radius. They clearly demonstrate the presence of a potential core in the throat section of the CSM, corresponding to normalized axial coordinates ranging from 4 to 6.

Another effect of the boundary layer is the reduction of the flux-averaged cross-sectional area of the venturi with respect to its geometrical area. This effect is particularly important in the diffuser, whose performance is very sensitive to even very small changes of the expansion ratio (see Figure 5). In theory it would be possible to compute the boundary layer displacement thickness for the assigned, nominal profile of the potential core velocity and to correct accordingly the venturi geometry. In practice this possibility should be regarded with some skepticism because boundary layer computations for flows with a highly unfavorable pressure gradient as the one in the diffuser are rather imprecise. Furthermore, it is questionable that their results could be accurately implemented in the manufacturing of small size venturis. However, if the results of these computations are to be trusted, in a venturi equal to the one previously considered but with a 20 mm long diffuser the presence of the boundary layer would, for example, increase the expansion ratio from its nominal value of 1.10 to a geometric value of 1.37.

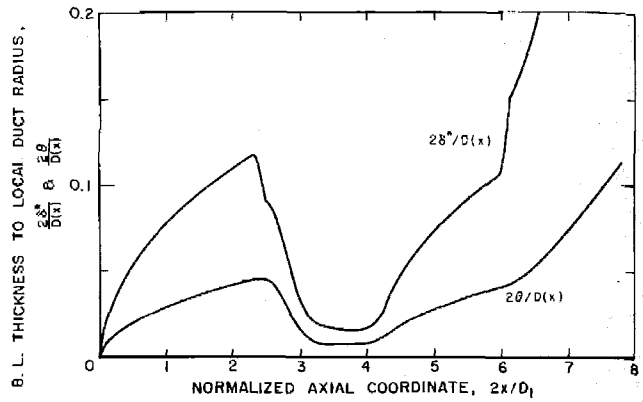

Fig. 9 Relative displacement thickness, $2\delta^*/D(x)$, and momentum thickness, $2\theta/D(x)$, v/s normalized axial coordinate $2x/D_i$ in a typical CSM venturi with D_i = 1 mm (throat diameter), C_c = 1/100 (contraction ratio), β_d = 0.76 deg (diffuser semi-aperture angle) and Re_i = 1400 (inlet Reynolds number). The lengths of the various sections are: L_i = 11.4 mm (inlet), L_c = 10.4 mm (contraction), L_t = 7.7 mm (throat), L_d = 10.4 mm (diffuser).

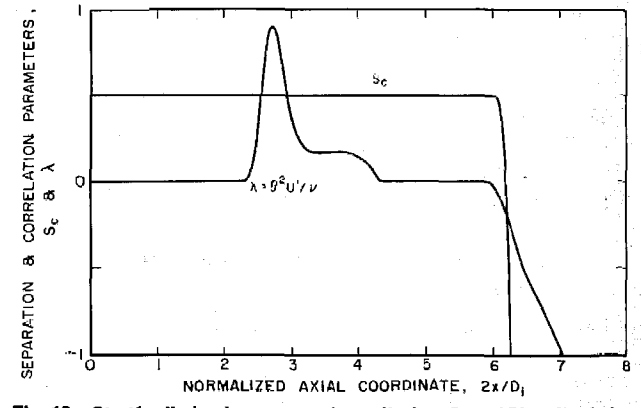

Fig. 10 Stratford's laminar separation criterion S_c and Thwaites' shear and shape correlation parameter $\lambda = \theta^2 U'/\nu$ v/s normalized axial coordinate $2x/D_i$ for the venturi of Fig. 9. Laminar separation is predicted when S_c drops to zero or $\lambda \simeq -0.09$.

Another problem to be expected in the venturi as a consequence of viscous effects is the occurrence of laminar separation in the diffuser when too large negative pressure gradients are present. If laminar separation takes place, cavitation nuclei from the main flow are likely to be trapped in the recirculation region, where they eventually grow and possibly develop into an attached cavity, whose unsteady behavior greatly disturbs the rest of the flow. The situation is further worsened if this cavity propagates downstream and reaches the exit. In this case the exhaust pressure is established throughout the cavity and the useful portion of the diffuser is proportionally shortened. A cylindrical section of appropriate length downstream of the diffuser promotes the stability of the exhaust flow and usually prevents the separation-cavitation from extending to the exit.

Preliminary tests on a prototype venturi and later experience with operational ones showed that steady or intermittent separation in the diffuser can indeed occur, a problem also reported by previous investigators (Oldenziel, 1982a; Shen et al., 1984). In view of this, the boundary layer correlation parameter $\lambda = \theta^2 U'/\nu$ (where U' is the streamwise derivative of the flow velocity at the boundary layer edge) and the Stratford laminar boundary layer separation criterion S_c (Stratford, 1954) have been plotted in Fig. 10. Separation is predicted when $\lambda = -0.09$ or $S_c = 0$. The two methods agree well with each other and also with the observed location of separation in the prototype venturi, thus indicating that less steep diffusers should be used, significantly limiting the minimum attainable throat pressure in the CSM venturi tube.

In view of the above considerations it was decided to develop a CSM with a transparent venturi tube where the throat velocity is measured by a LDV and the upstream pressure by an absolute pressure transducer. At the same time the LDV signal will also be used to detect the occurrence of cavitation at the throat of the venturi tube. The analysis of the signals from the LDV and the upstream pressure transducer will be carried out by an especially designed electronic Signal Processor for real time generation and temporary storage of the relevant data. Finally, the final acquisition and reduction of the data will be performed by a microcomputer.

5 LDV Optical Analysis and Signal Processing

In this section the main considerations and electro-optical analysis are presented which led to the design of the LDV used in the CSM. These considerations mostly concern the choice of the optical configuration and the connected problem of the LDV signal processing. Basic principles of operation of LDV's are recalled as required for clarity of the presentation, but for more details the reader is referred to the vast literature available on this complex field (see, for example, Durst et al. 1981).

The typical optical properties of the LDV scatterers naturally present in the CSM flow cannot be anticipated with any degree of accuracy, since they depend on the individual characteristics of the sampled water and no artificial seeding can be used without greatly interfering with the water quality measurement. However, cavities will clearly be present at the end of the venturi throat section as long as measurements with the CSM can be made. Since the pressure gradient in the venturi throat is ideally zero, it can be shown that the slip velocity of the two phases nearly vanishes at the end of the throat section and the cavities themselves can therefore be safely used as velocity tracers. The possibility of recording the velocity of cavities in the flow also provides useful information on their origin. In fact, since the typical cavity size is much larger than the boundary layer thickness at the CSM throat, the cavities generated by free stream nuclei mostly travel at the potential core speed, while those just released by nearby surface nuclei are significantly slower. A dual beam back-scattering LDV focused at the end of the venturi test section that uses the cavities themselves as tracers has therefore been selected for measuring the CSM throat velocity. The back-scattering configuration combines the advantages of greater simplicity with superior optical efficiency when operating in the scattering regime expected from cavities whose average size clearly much exceeds the wave length of the illuminating laser beams.

For this arrangement the Doppler frequency of the LDV signal, the fringe spacing and the number of fringes are respectively expressed by:

$$f_D=\frac{2Um\sin\varphi}{\lambda_0};\quad s_{fr}=\frac{\lambda_0}{2m\sin\varphi};\quad N_{fr}=\frac{d_x}{s_{fr}}=\frac{d_x f_D}{U}$$

where φ is the semi-aperture angle of the two intersecting beams, λ_0 is the wave length of the beams in air, m is the index of refraction of the optical medium, U is the velocity component perpendicular to the optical axis in the plane of the two beams, and d_x is the size of the LDV probe volume in the flow direction.

The Doppler frequency and the fringe spacing are not affected by the refraction of the two beams through a plane interface separating two optical media with index of refraction m and m', because in this case from Snell's law: $m\sin\varphi = m'\sin\varphi'$, where φ' is the beam semi-aperture angle in the second medium. This result can be easily generalized to the case of a sequence of planar, parallel interfaces. Also note that the Doppler frequency is only sensitive to the orientation of the impinging radiation in the plane of the two beams, which coincides with the meridional plane of the CSM venturi. Within the limits of Gaussian or paraxial optics the effects due to the cylindrical geometry of the venturi optical interfaces can be separately analyzed in the meridional and cross-sectional planes. The curvature of these interfaces in the cross-sectional plane therefore refracts the impinging beams in the same plane, but has no effect on the direction of the beam propagation in the meridional plane. The above considerations imply that the LDV Doppler frequency only depends on the venturi geometry in the meridional plane and that its relation to the velocity is the same in air and in the CSM flow, provided that the walls of the venturi are parallel. This is a very fortunate situation, since it implies that the calibration of the LDV can be carried out in air and that its results can be directly extended to the flow in the CSM venturi.

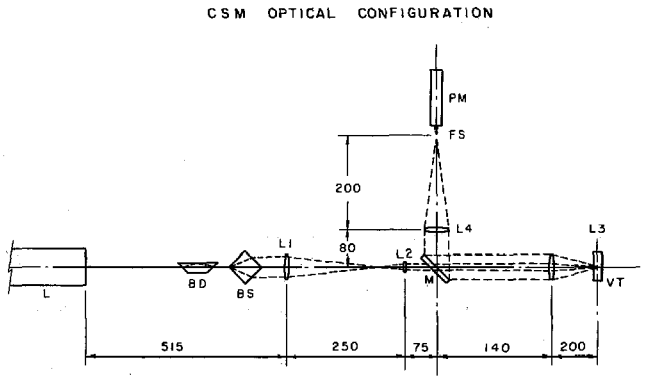

Fig. 11 Schematic for the CSM optical components (dimensions in mm): continuous wave laser (L), beam displacer (BD), beamsplitter cube (BS), telescopic relay lenses (L1 and L2), focusing and receiving lens (L3), venturi tube (V), front surface mirror (M) with slit for transmission of laser beams, photomultiplier collimating lens (L4), field stop aperture (FS), photomultiplier tube (PM).

As mentioned earlier, in the CSM it is highly advisable to preserve the information on the occurrence time of individual cavitation events. In addition, the drop-out rate and the signal level are expected to be high, since the cavities used as velocity tracers are relatively sparse and large. Therefore frequency counters, which operate in the time domain, are the most suitable solution for measuring the LDV Doppler frequency. Each burst is recognized, isolated, and its Doppler frequency is counted by comparing the LDV signal to properly adjusted threshold levels. On the other hand, with respect to alternative methods, in frequency counters the maximum measurable frequency is more severely limited by the speed of the processing electronics and therefore the LDV optics must be designed accordingly.

The best LDV signal quality is obtained when the fringe spacing is of the same order of magnitude as the size of the scatterer, whose characteristic dimensions cannot be safely anticipated. It seems therefore advisable to keep the beam separation adjustable within a relatively large range. The above consideration and the need to limit the Doppler frequency below about 1 MHz in order to simplify the LDV processing electronics led to the arrangement schematically shown in Fig. 11. The laser beam, generated by a 5 mw He-Ne continuous wave laser (L), goes through a beam displacer (dove prism, BD) and a metal-coated beamsplitter cube (BS). The separation of the two outcoming beams can be widely adjusted (2 to 17 mm ca.) using the beam displacer to change the transversal position of the beam entering the beamsplitter. In order to reduce the Doppler frequency of the LDV signal and consequently simplify the processing electronics, the beam separation is then four times reduced by a telescopic lens relay (L1 and L2). After passing through a slit in the front surface mirror (M), the two beams are finally focused by the lens (L3) to the test section of the CSM venturi tube (VT). The back-scattered light is then collected by the whole aperture of the same lens (L3) and mostly reflected by the front surface mirror (M)

toward the photomultiplier collimating lens (L4). The resulting image of the test section is filtered by a field stop aperture (FS) to reduce the optical background noise and finally reaches the photomultiplier tube (PM), where it is converted into an electric signal. All lenses have a back focal length of 200 mm, except the second lens (L2) of the telescopic relay, whose focal length is 50 mm.

Since the deviation of the laser beams from the optical axis is small, the theory of propagation of paraxial Gaussian beams can now be used to analyze the optical system in order to deduce the focal volume and the expected number of fringes of the LDV signal. Then, for the system of thin lenses of Fig. 11, the ray transfer matrices (Kogelnik and Li, 1966) of the focusing optics from the laser window to the LDV focal point and of receiving optics from the LDV focal point to the photomultiplier are respectively:

$$\underline{A}_F = \begin{bmatrix} 0 & -0.8 \\ 1.250 & -0.3063 \end{bmatrix}; \quad \underline{A}_R = \begin{bmatrix} -1 & 0 \\ -4.5 & -1 \end{bmatrix}$$

where the optical lengths are in meters. The elements a_{11} and $-a_{21}$ of these matrices are, respectively, the magnification and the reciprocal of the back focal length of the optical system. As expected, the magnification of the receiving optics is equal to -1. Furthermore, the ray transfer matrix of the focusing optics shows that, for the flow velocity expected at the venturi throat ($U \simeq 15$ m/s), the Doppler frequency can be decreased to less than 250 kHz with a beam separation of a few millimeters, still large enough to be achieved with a cube beam-splitter.

In the theory of paraxial optics the propagation of a Gaussian beam is expressed in terms of the complex beam parameter (Kogelnik and Li, 1966):

$$\frac{1}{q} = \frac{1}{R} - i\frac{\lambda}{\pi w^2}$$

where $1/R$ is the beam wave front curvature and w is the beam radius, defined as the distance from the beam axis where the electromagnetic field amplitude drops to $1/e$ times its maximum value. At the beam waist the wave front curvature is zero and the beam radius is minimum. The size and location of the beam waist depend on the internal geometry of the laser optics. In the Spectra Physics He-Ne gas laser model Stabilite 120 to be used in the CSM the beam waist radius is $w_0 = 0.325$ mm and coincides with the output window of the laser. In the propagation of a Gaussian beam through an optical system with ray transfer matrix $\underline{A}$ the complex beam parameter at the output q_2 is related to the input value q_1 by (Kogelnik and Li, 1966):

$$q_2 = \frac{a_{11}q_1 + a_{12}}{a_{21}q_1 + a_{22}}$$

From this equation and the above results the beam radius and the curvature of the wave front at the LDV focal point are: $1/R_f = 0.383\ \text{m}^{-1}$ and $w_f = 0.496$ mm. In the final operational configuration of the LDV the beam angular semi-separation is $\varphi = 5.27 \cdot 10^{-3}$ rad and the fringe spacing $s_{fr} = 60\ \mu$m, which experience has shown to give the best results. With this choice the axes of the LDV focal ellipsoid are: $d_x = 2w_f/\cos\varphi = 0.992$ mm in the flow direction, $d_y = 2w_f/\sin\varphi = 188$ mm in the direction of the optical axis, $d_z = 2w_f = 0.992$ mm in the vertical direction. Then the number of fringes and the duration (gate time) of a typical Doppler burst can be estimated to be $N_{fr} = d_x/s_{fr} \simeq 17$ and $T_g = d_x/U \simeq 66\ \mu$s. Clearly the fringe spacing must be as uniform as possible throughout the LDV focal volume in order to obtain consistent velocity readings regardless of the location of the scatterer trajectory. For this to happen the beam divergence angle $w_f/R_f = 1.90 \cdot 10^{-4}$ rad must be much smaller than the angular semi-separation φ between the two beams. This condition is indeed satisfied in the configuration examined here. Finally, the magnification of the receiving optics is equal to -1 in the meridional plane and slightly larger in the cross-sectional plane as a consequence of the curvature of the venturi tube interfaces. Thus, the optimum diameter of the photomultiplier field stop aperture should be about 1 mm or a bit larger, as confirmed in practice.

Note that for a throat diameter $D_t = 1$ mm the LDV focal volume extends far across the venturi walls in the direction of the optical axis and also covers the whole throat in the vertical direction. Therefore the LDV signal can effectively monitor the occurrence of cavitation, but at the same time velocity readings in the boundary layer are likely to occur. This situation must be taken into account in the reduction of the LDV data in order to introduce the appropriate corrections when necessary. The occurrence of velocity readings in the boundary layer also provides a direct way to check for the presence of a potential core in the flow at the venturi throat, which is essential for the correct deduction of the throat pressure.

In theory the intensity of the LDV output signal could now be estimated from the laser power, the transmittance of the optical system, the focal point dimensions and the photomultiplier's sensitivity. However, in practice the scattering and collecting efficiencies are too uncertain for a useful estimate to be made because they depend in a very complex way on the optical and geometrical properties of both the tracer itself and of the collecting optics.

6 Summary and Conclusions

The results of design analysis of the CSM operation can be summarized as follows:

- the flow is likely to remain laminar throughout the venturi's throat section and the first portion of the diffuser;
- the existence of a potential core at the throat has been demonstrated in venturi tubes of proper geometry by estimating the boundary layer thickness;
- the pressure in the CSM cavitation region is an extremely sensitive parameter and cannot be measured directly with the necessary accuracy;
- the indirect measurement of the pressure in the cavitation region appears to be best accomplished by measuring the upstream pressure with an absolute pressure transducer and the potential core velocity at the CSM throat with non-intrusive direct methods such as a LDV;
- the detection of cavitation at the venturi throat is best accomplished optically by the same LDV signal used to measure the flow velocity;
- it is clearly advantageous for the purpose of monitoring the flow to preserve the optical access to the cavitation region whenever possible;
- the errors and limitations due to nuclei interference effects can be effectively controlled by decreasing the volume of the cavitation region to less than ten cubic millimeters;
- for a throat diameter of 1 mm the time response of the cavitating nuclei imposes a lower bound of about 5 to 10 mm to the length of the CSM throat section;
- the flow is extremely sensitive to laminar separation in the diffuser, which limits the maximum achievable expansion ratio to less than 1.1;
- the acquisition system must be designed to handle up to ten thousand events per second, recording for each of them the occurrence time, the Doppler frequency and the upstream pressure;
- a dual-beam back-scattering LDV seems to be the most suitable solution for measuring the CSM throat velocity and monitoring the occurrence of cavitation;
- it is advisable to keep the fringe spacing widely adjustable in order to optimize the LDV signal visibility and Doppler frequency depending on the operational conditions;

- the Doppler frequency must be measured in the time domain with a frequency counter in order to record both the velocity and the occurrence time of individual cavitation events;
- the Doppler frequency should not exceed about 1 or 2 MHz due to likely limitations of the processing electronics;
- spurious velocity readings from scatterers convected in the boundary layers must be eliminated in the reduction of the data.

In conclusion, the above analysis provides a rational basis and strong indications for CSM design orientation. It clearly shows that proper CSM operation poses a relatively complex technological problem, where a number of critical factors are involved. In the proposed configuration, the solution of this problem requires the integration of both fluid dynamic and electro-optical aspects. The above analysis indicates that, by careful consideration of these aspects, a CSM capable of measuring the concentration of active cavitation nuclei as a function of the throat pressure can be successfully developed according to the proposed design. As mentioned in the introduction, the implementation and operation of this system are described and discussed in a companion publication (d'Agostino and Acosta, 1991).

Acknowledgments

This research has been funded by the Office of Naval Research and by the Naval Sea Systems Command General Hydromechanics Research Program administered by the David W. Taylor Naval Ship Research and Development Center. The North Atlantic Treaty Organization—Consiglio Nazionale delle Ricerche, Italy, has also contributed to the support of this work through a 1982 and a 1983 Fellowship for Technological Research. Special thanks to Dr. T. T. Huang of DTNSRDC for his interest in this work, to Mr. Joe Fontana, Mr. Elton Daly, Mr. Rich Eastvedt, Mr. Leonard Montenegro, Mr. John Lee and to Miss Cecilia Lin of the Caltech staff for their assistance in the completion of the experiment and to Dr. Haskel Shapiro, Mr. Bob Kirkpatrick and their group for the design and implementation of the custom-made electronics.

References

Bader, H., 1970, "The Hyperbolic Distribution of Particle Sizes," *Journal of Geophysical Research*, Vol. 75, No. 15, pp. 2822-2830.

Billet, M., 1986a, "The Importance and Measurement of Cavitation Nuclei," *Advancements in Aerodynamics, Fluid Mechanics and Hydraulics*, Minneapolis, Minn., pp. 967-989.

Billet, M., 1985, "Cavitation Nuclei Measurement—A Review," *ASME Cavitation and Multiphase Flow Forum*, Albuquerque, N.M., pp. 31-38.

Browlee, K. A., 1960, *Statistical Theory and Methodology in Science and Engineering*, Wiley, NY.

Chahine, G. L., and Shen, Y. T., 1986, "Bubble Dynamics and Cavitation Inception in Cavitation Susceptibility Meters," ASME JOURNAL OF FLUIDS ENGINEERING, Vol. 108, pp. 444-452.

d'Agostino, L., 1987, "Experimental and Theoretical Study on Cavitation Inception and Bubbly Flow Dynamics," Ph.D. thesis, Report No. Eng. 183.16, California Institute of Technology, Pasadena, Calif.

d'Agostino, L., and Acosta, A. J., 1991, "A Cavitation Susceptibility Meter with Optical Cavitation Monitoring—Part Two: Experimental Apparatus and Results," published in this issue pp. 270-277.

d'Agostino, L., Thai Pham, and Green, S., 1989, "Comparison of a Cavitation Susceptibility Meter and Holographic Observation for Nuclei Detection in Liquids," ASME JOURNAL OF FLUIDS ENGINEERING, Vol. 111, No. 2, pp. 197-203.

Durst, F., Melling, A., and Whitelaw, J. H., 1981, *Principles and Practice of Laser-Doppler Anemometry*, Academic Press, 2nd edition.

Godefroy, H. W. H. E., Jansen, R. H. J., Keller, A. P., and van Renesse, R. L., 1981, "Comparison of Measuring and Control Methods of the Water Quality with Respect to Cavitation Behaviour," Delft Hydraulics Laboratory Publication.

Ito, Y., and Oba, R., 1980, "Cavitation Observations through a Fine Laser-Beam Technique," Report No. 337, Institute of High Speed Mechanics, Tohoku University.

Knapp, R. T., Daily, J. W., and Hammitt, F. G., 1970, *Cavitation*, McGraw-Hill, New York.

Kogelnik, H., and Li, T., 1966, "Laser Beams and Resonators," *Applied Optics*, Vol. 5, No. 10, pp. 1550-1567.

Lecoffre, Y., and Bonnin, J., 1979, "Cavitation Tests and Nucleation Control," *International Symposium on Cavitation Inception*, New York, New York, pp. 141-145.

Le Goff, J. P., and Lecoffre, Y., 1983, "Nuclei and Cavitation," *14th Symposium on Naval Hydrodynamics*, National Academy Press, pp. 215-242.

Oba, R., Ikohagi, T., and Kim, K. T., 1979, "Cavitation in an Extremely Limited Flow through Very Small Orifices," *International Symposium on Cavitation Inception*, ASME, New York, N.Y., pp. 147-152.

Oldenziel, D. M., 1982a, "A New Instrument in Cavitation Research: the Cavitation Susceptibility Meter," ASME JOURNAL OF FLUIDS ENGINEERING, Vol. 104, pp. 136-142.

Oldenziel, D. M., 1982b, "Utility of Available Instruments during Cavitation Tests," *Proceedings of Symposium on Operating Problems of Pump Stations and Power Plants*, IAHR, Amsterdam.

Oldenziel, D. M., 1979, "New Instruments in Cavitation Research," *International Symposium on Cavitation Inception*, New York, N.Y., pp. 111-124.

Oldenziel, D. M., Jansen, R. H. J., Keller, A. P., Lecoffre, Y., and van Renesse, R. L., 1982, "Comparison of Instruments for Detection of Particles and Bubbles in Water during Cavitation Studies," *Proceedings of Symposium on Operating Problems of Pump Stations and Power Plants*, IAHR, Amsterdam.

O'Hern, T. J., d'Agostino, L., and Acosta, A. J., 1988, "Comparison of Holographic and Coulter Counter Measurements of Cavitation Nuclei in the Ocean," ASME JOURNAL OF FLUIDS ENGINEERING, Vol. 110, pp. 200-207.

Plesset, M. S., and Prosperetti, A., 1977, "Bubble Dynamics and Cavitation," *Ann. Rev. Fluid Mech.*, Vol. 9, pp. 145-85.

Shen, Y. T., Gowing, S., and Pierce, R., 1984, "Cavitation Susceptibility Meters by a Venturi," *International Symposium on Cavitation Inception*, ASME Winter Annual Meeting, pp. 9-18.

Shen, Y. T., and Gowing, S., 1985, "Scale Effects on Bubble Growth and Cavitation Inception in Cavitation Susceptibility Meters," *ASME Cavitation and Multiphase Flow Forum*, Albuquerque, New Mexico, pp. 14-16.

Shen, Y. T., Gowing, S., and Eckstein, B., 1986, "Cavitation Susceptibility Measurements of Ocean Lake and Laboratory Waters," David W. Taylor Naval Ship Research and Development Center, Report DTNSRDC-86/D19.

Stratford, B. S., 1954, "Flow in Laminar Boundary Layer near Separation," Aeronautical Research Council, R&M 3002.

White, F. M., 1974, *Viscous Fluid Flow*, McGraw Hill, New York.